ACADEMIC PRESS

Available online at www.sciencedirect.com
SCIENCE DIRECT®

Journal of Solid State Chemistry 171 (2003) 76–83

JOURNAL OF SOLID STATE CHEMISTRY

http://elsevier.com/locate/jssc

Transport properties and magnetoresistance of La–Ca manganites near the optimal doping concentrations

M. García-Hernández,* A. de Andrés, J.L. Martínez, D. Sánchez Soria, L. Martín-Carrón, and S. Taboada

Instituto de Ciencia de Materiales de Madrid, Consejo Superior de Investigaciones Científicas (CSIC), Cantoblanco, E-28049 Madrid, Spain

Received 17 May 2002

Abstract

We review our work on the characterization and modeling of the extrinsic and intrinsic contributions to the magnetoresitance of La–Ca manganites near the optimal doping. Firstly, we propose a macroscopic model for the electronic transport that parametrically quantifies the intrinsic and extrinsic contributions to the magnetoresistance, when grain boundaries are present. Then, we complete this model by considering the effects of Coulomb blockade in the electronic transport at low temperatures in polycrystalline samples. Secondly, we explore at a microscopic scale the existence of intrinsic inhomogeneities and the possibility of controlling the electron–lattice coupling by introducing controlled chemical defects. Finally, we describe the effects that these artificially built-in barriers have on the magnetoresistive properties of the system at very low magnetic fields.
© 2003 Elsevier Science (USA). All rights reserved.

Keywords: Colossal magnetoresistance; Manganites; Magnetic; Electronic transport; Structural properties; Thin films

1. Introduction

Rare-earth (R)-doped manganites with general formula $R_{1-x}A_xMnO_3$, where A is an alkaline earth cation, show an intricate phase diagram with a broad phenomenology [1] that, depending upon the level of doping and some structural parameters, ranges from ferromagnetic (FM) to antiferromagnetic (AF) interactions and from metallic or semiconductor behavior to charge ordered insulators.

La–Ca compounds with $0.15<x<0.5$ present a metal insulator transition, at T_{MI}, and a paramagnetic (PM) to FM ordering, at T_c, both about 265 K for $x=0.33$, the region near the optimum doping where T_c is close to room temperature and reaches its maximum for this series. This makes optimal doped compounds particularly interesting from the application point of view, since intrinsic magnetoresistance effects are associated to the above-mentioned transitions. This intrinsic magnetoresistive behavior have been understood in terms of the double exchange mechanism describing the FM metallic state plus the strong phonon–electron coupling, particularly relevant in the insulator regime, where the conduction is achieved by hopping of small polarons. Also, within the basic framework of a double exchange mechanism plus an electron–phonon interaction, recent theoretical developments start to draw a unified picture of the whole $R-A$ perovskites series. The proposed scenario confers a prominent role to the strong tendency towards phase separation exhibited by these systems and caused by intrinsic inhomogeneities [2]. The particular transport and magnetic properties of a given composition would be then determined by the specific equilibrium sustained between competing segregated domains: typically FM metallic, AF orbital or charge ordered, and PM insulating patches [2]. Within this framework, polarons would play the role of inhomogeneities and the magnetoresistive properties would be also explained as a result of altering the initial equilibrium between phases. In particular, for the $x=0.33$ La–Ca compound, the applied magnetic field would reinforce and enlarge the FM and metallic domains at the expense of the insulating ones (PM), therefore inducing the observed colossal magnetoresistance effect.

In addition to these intrinsic magnetoresistive effects, extrinsic effects are of paramount importance since they

*Corresponding author. Fax: +34-91-172-06-23.
E-mail address: marmar@icmm.csic.es (M. García-Hernández).

0022-4596/03/$ - see front matter © 2003 Elsevier Science (USA). All rights reserved.
doi:10.1016/S0022-4596(02)00191-3

are responsible for the large values of the magnetoresistance observed at low magnetic fields. Such effects are known to be due to spin-dependent scattering process at the grain boundaries, artificially built-in frontiers, microcracks and mesoscopic and macroscopic defects.

In this paper, we review our work on the characterization and modeling of the extrinsic and intrinsic contributions to the magnetoresistance of these systems. Firstly, we propose a macroscopic model for the electronic transport that parametrically quantifies the intrinsic and extrinsic contributions to the magnetoresistance [3–5], when grain boundaries are present. Then, we complete this model by considering the effects of Coulomb blockade (CB) in the electronic transport at low temperatures in polycrystalline samples [6]. Secondly, we will explore at a microscopic scale the effect of intrinsic inhomogeneities [7] and the possibility of controlling the electron–lattice coupling by introducing controlled chemical defects [8]. Finally, we describe the effects that these artificially built-in barriers have on the magnetoresistive properties of the system at very low magnetic fields.

2. A macroscopic model for electronic transport: intrinsic and extrinsic effects

We have measured the magnetic and transport behavior of two sets of ceramic pellets with the same grain size (several microns). Both series were prepared as follows: One-half of the available $La_{0.7}Ca_{0.3}MnO_3$ (LCMO) powder was annealed at 1200°C for 24 h to clean the surface of the grains. The pellets obtained from this powder are labeled C (clean). The other half of the powder was stored in air for several weeks (samples labeled D for dirty surface) in order to degrade the surface of the grains by absorbing CO_2 and water. With each kind of powder we conform four pellets by sintering for 4 h at different temperatures: 200°C, 500°C, 800°C and 1100°C for 4 h. Samples were fully characterized from the structural, magnetic and transport points of view. The magnetic transition temperature, T_c, is identical for all the samples, whether they are dirty or clean samples. However, as seen in Fig. 1, the normalized resistance and the magnetoresistive ratios present severe differences not only between both series, but also within the same series, depending on the annealing temperature.

Our phenomenological model for the electronic transport proposes the existence of two kinds of channels connected in parallel (Fig. 2). One kind is related to the intrinsic transport properties of the system, their resistance does not depend on the connectivity of the sample and are dominant between well-connected grains. The other kind of channels present energy barriers to electronic transport that behave as capacitors and inhibit metallic conduction at all temperatures, due to poor connectivity, disorder or contamination at the grain surfaces. This model leads to the following expressions that reproduces the measured resistance (see Fig. 1):

$$1/R = (S_m/\rho_m + S_i/\rho_i),$$

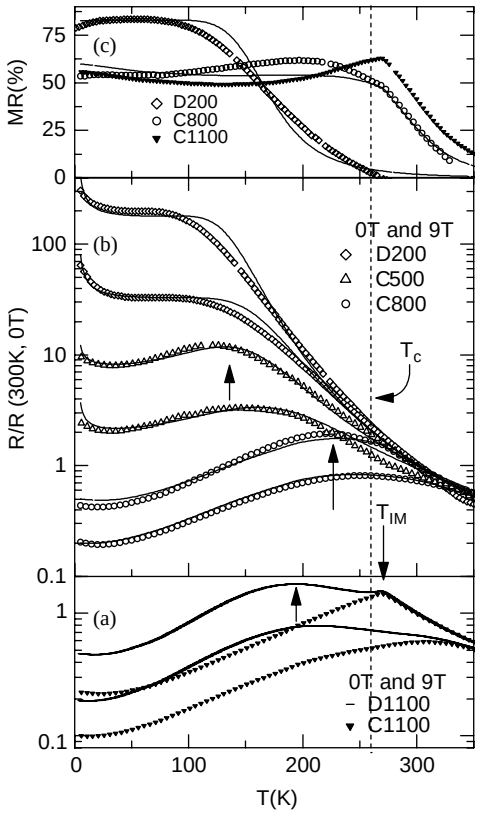

Fig. 1. Normalized resistance at 0 and 9 T for (a) two pellets, both annealed at 1100°C but with "clean" (C1100) and "dirt" (D1100) starting powders showing the effect of a dirt surface in the resistance; (b) pellets annealed at different temperatures (200°C, 500°C, 800°C and 1100°C); and (c) magnetoresistance for three samples. Continuous lines are the fits detailed in the text.

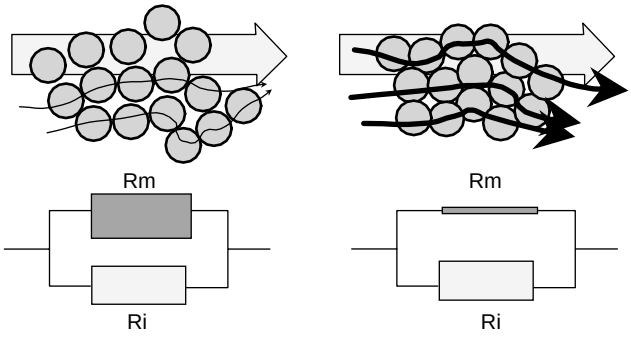

Fig. 2. Schema for the conduction in two granular systems with a poor connectivity (left) and a better connectivity (right). Lower part: the equivalent circuits with two resistances in parallel: R_M (for good channels) and R_I (for bad channels). Curved arrows in the upper part are related to good channels.

where ρ_m stands for the intrinsic resistivity of the channels that, as expected from a double exchange system, become metallic below T_c and ρ_i is the resistivity corresponding to the channels that, due to the presence of extrinsic defects or boundaries are insulators with an activation energy E_i. S_m and S_i are the respective effective sections for each sort of channel. ρ_m should correspond to the resistivity of a quality single crystal but for this study we take $\rho_m(T) = \rho(C1100, T) + A\exp(E_a/k_bT)$, i.e., the resistivity of our best powdery sample, in series with a component that takes into account the low temperature (below 50 K) increase of the resistance. We will show that this latter component is due to charging effects that can rigorously be taken into account by a renormalized CB model. The insulating paths with resistivity ρ_i are simply modeled by a semiconductor-like resistivity: $\exp(E_i/K_BT)$ with $E_i = 100$ meV (the activation energy usually reported for the PM phase). Continuous lines in Fig. 2 show the best fit for several samples at 0 and 9 T, where the only fitting parameters are S_m/S_i and A. The activation energies being the same for all the samples. Note that, in order to fit the 9 T measured resistance we only modify the ratio of the effective sections of metallic and insulating channels (S_m/S_i).

Common feature of all these polycrystalline samples is the existence of two different regimes in the field dependence of the magnetoresistance, as can be easily spotted in Fig. 3. At low temperatures and low field (the steep slope region in Fig. 3), up to near the fully magnetization of the sample, the chief process in the electronic transport is the spin polarized tunneling at grain boundaries [9] which, in turn, depends on the relative orientation of the magnetic moments of the grains. Therefore, the magnetoresistance at low fields, basically follows the measured magnetization. Simultaneously, when the magnetization has technically reached saturation, the progressive ordering of just a few Mn spins blocked at the grain surface switch on new channels for metallic conduction, as the field increases, that work in parallel to those already conducting at zero field. The latter effect explains the progressive and smooth decrease of the resistance in the high-field region. The main hypothesis of our model is that the opening of these new conducting channels is proportional to the applied field ($S_{new} = fH$). Following these lines, we have developed a model for the magnetic field dependence of the magnetoresistance that with just one fitting parameter (f/S_m) fits the measured values, as it is described in detail in Ref. [3]

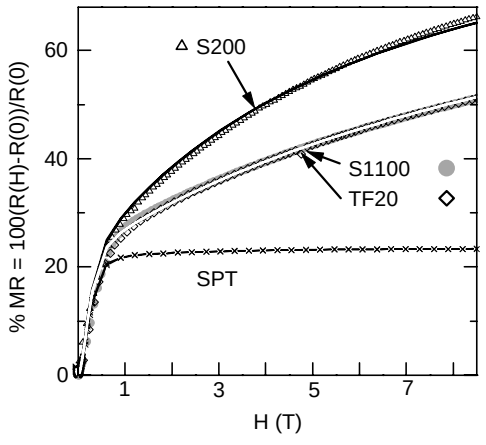

Fig. 3. Magnetoresistance of C1100 and D200 pellets and TF20 thin film (gray symbols). Crosses are the magnetoresistance obtained from the measured magnetization of a pellet and continuous lines (black and white) are the fits to the magnetoresistance of three samples.

Following these lines, we have also demonstrated that the field dependence of the magnetoresistance at a fixed temperature, MR(H), can be expressed as

$$\mathrm{MR}(H) = 100[R_g(H)/R_g(0) - 1]$$

with

$$R(H)/R(0) = 1/[1 + (C/\sigma_g(0))\,(M(H)/M_s)^2] \times [1 + fH/S_m)],$$

where σ_m is the conductivity for the good metallic channels (intrinsic), M_s and $M(H)$ is the saturated magnetization for the sample and the field-dependent magnetization, respectively, and C is a constant for a given temperature. S_m is the effective section for the good conducting channels and the only fitting parameters are C/S_m, that is fixed for all compounds to 0.33, and f/S_m.

A further proof of the crucial role of the extrinsic (connectivity effect) in the electronic transport of manganites is provided by the frequency dependence of the modulus of the complex AC impedance Z, as shown in Fig. 4. The observed decrease for the sample that has been annealed at 200°C is reproduced using a pure resistance and capacitor in parallel as the equivalent circuit. This behavior is not observed for the sample annealed at 1100°C, whose resistance is independent of the frequency. This behavior can be explained taking into account that, for poorly connected samples, carriers are localized within the grains since, in order to overcome the intergrain barriers, some energy is required but not available at low temperatures. Consequently, the measured impedance decreases as the frequency increases since the carriers can follow the AC field within a grain without need to cross over the intergranular barriers. The barrier to intergrain conduction are higher for samples badly connected (sintered at lower temperatures). For the high-temperature annealed sample, we do not see this effect since it is macroscopically well connected and carriers do not localized within the grains. This picture should be valid for all kinds of artificial boundaries, like grains, scratches, microcracks, etc.

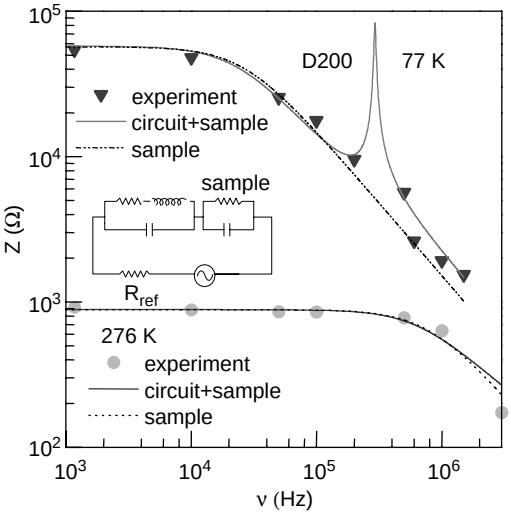

Fig. 4. Frequency dependence of the impedance modulus at low (77 K) and high (276 K) temperature of the D200 pellet. The inset shows the equivalent circuit of the sample (capacitor and resistance) and of the experimental setup.

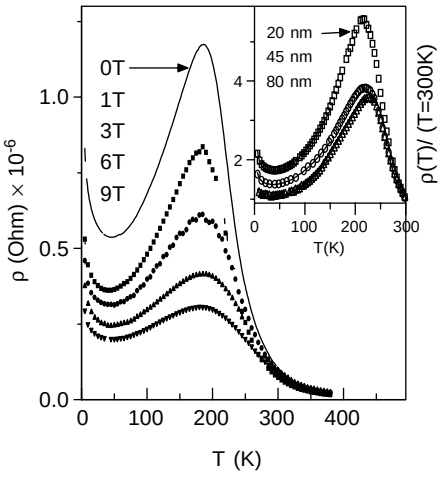

Fig. 5. Resistance vs. temperature for the smallest particle size explored (grain diameter = 12 nm) at several magnetic fields. Inset: resistance vs. temperature for other films in the series at 0 T. Continuous lines are best fit to the data.

3. Extrinsic charging effects in the electronic transport of manganites

As already mentioned, charging effects are important for small grain size polycrystalline samples. It is well established that the electrical conduction in granular metals results from the transport of electrons or holes from charged to neutral grains. This requires the generation of a charge carrier by removing an electron from a neutral grain and placing it in a neighboring neutral grain, some electrostatic energy being involved in the process, the so-called charging energy E_c. As the temperature decreases or the grain size decreases, it is increasingly difficult to activate the electronic transport and this situation may evolve to a point in which the transport could be effectively blocked (CB).

We have measured and modeled these effects for a set of thin films of LCMO with grain sizes in the nanometric lengthscale. Fig. 5 shows the resistance for different magnetic fields corresponding to our smallest grain size film (diameter = 12 nm). The inset shows also the resistance at zero field normalized to the room temperature value for representative films in the set. All of them share the same basic features: a neat MI transition at a temperature slightly below the FM transition, as expected for a bulk manganite [1], and an upturn of the resistance that starts to develop below 40 K, that could be assigned to the existence of a Coulomb gap. The latter being more prominent as the grain size diameter of the sample decreases. As expected, a decrease of the resistance is observed upon application of an external magnetic field.

In order to get some insight into the physics of the low-temperature behavior of the resistance we have analyzed, the portion of the curves, up to $T = 150$ K, as the sum of two contributions $R(T) = AR_0 + B_{\exp}(\Delta/T)^{1/2}$ where R_0 stands for the resistance of the bulky target, which does not present the upturn below 40 K, and A is an amplitude factor. Regarding the exponential contribution, we mention that fits improve assuming a $T^{-1/2}$ dependence in the argument of the exponential instead of the T^{-1} dependence postulated for a pure CB effect. B is an amplitude factor and Δ is a fitting parameter that is related to the charging energy E_c.

The model reproduces the data below 150 K, as can be seen in the inset of Fig. 2 where the fitted line lays below the experimental points.

In order to give account of the strong variation with the applied field is observed in the low-temperature upturn of the resistance, which is not expected for a pure CB process, we have extended the standard CB model developed by Helman and Abelles in the early seventies [10], along the lines given in Ref. [6]. Our model keeps the charging energies constant while enhancing the coupling between grains, leading to a delocalization of the charges to neighboring grains, as the applied field increases. The outcome of this process can be understood as a reduction in the effective capacitance of the grains by the applied field that, as seen in Fig. 6, follows an exponential function.

4. Intrinsic inhomogeneities at nanoscopic scales

As already mentioned, due to the strong interplay between magnetic, lattice and electronic degrees of freedom in manganites, the existence of non-homogenous states in manganites is put forward by the most recent theories. In particular, the equal electronic

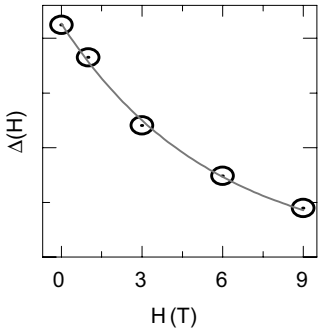

Fig. 6. Magnetic field dependence D for the film with grain diameter 12 nm. The full line shows the fit to an exponential function.

density phase separation induced by disorder would configure a mixed phase scenario around a first-order metal–insulator (MI) transition in the intermediate hole doping range. Here the level of disorder is the chief variable defining the length scale of each phase.

$La_{2/3}Ca_{1/3}MnO_3$ (LCMO) appears to be a good realization of a system where disordered induced phase separation may take place. Non-homogenous states have been inferred in LCMO from different experiments [11–12] but all lacking a microscopic description of the inhomogenities. In order to get such a description of the inhomogeneous state, we have combined neutron powder diffraction techniques and reverse Monte Carlo (RMC) [13] modeling of the Bragg (nuclear and magnetic) and diffuse scattering intensities. The main novelty of this approach is the feasibility to find local departures from the single cell description of the crystalline and magnetic structures. Detailed account of the experiments and simulations can be found in Ref. [7]. It has been found that distortions with respect to the averaged *Pnma* structure exist and are basically localized within the (a,c)-plane of the perovskite. Also, the analysis of the magnetic intensities draws an inhomogeneous scenario in which three different phases coexist (FM and AF domains within a PM matrix) in LCMO near T_{MI}. This microsegregation is probably driven by the distortion in the positions of the Mn atoms within the (a,c) plane that develops around T_c and T_{MI}. As a result, there are Mn atoms whose distance to the nearest-neighbor Mn atom is shorter than that corresponding to the averaged structure. These atoms present also shorter Mn–O distances and above T_c hold short-range FM interactions within the PM matrix.

As the temperature decreases below T_c, these FM clusters increase their coherence length and the matrix becomes FM. Also, within the (a,c) plane we have found a significant number of Mn atoms separated from their Mn nearest neighbors a distance longer than the averaged Rietveld distance. These pairs (about 15% of the nearest neighbors at 280 K) interact AF around T_c and display longer Mn–O distances making double exchange less efficient, as overlap decreases. The temperature dependence of the FM and AF correlations is given in Fig. 7 where a correspondence with the local distortion of the octahedra can be easily seen. It is worth mentioning that the AF domains show a phenomenology similar to that reported for the CE state in $La_{0.5}Ca_{0.5}MnO_3$ near the Neel temperature [14], making plausible to identify these islands as probable precursors of the CE phase.

Note also, Fig. 7, that the onset of the metallic state does not occur until the AF correlations considerably weaken, pointing out that the AF entities act as strong electron scatterers that add extra restrictions to the electron transport in the PM phase. It is realistic also to think that the application of an external field would inhibit the formation of this exotic AF phase resulting in the decrease of the electron scattering and lowering the resistivity.

5. Raman phonons—intrinsic inhomogeneities and microphases

Theories converge in the necessity to include electron–lattice interactions, which are able to localize the carriers into small polarons through their coupling to lattice distortions, disorder or phonons. The involved phonons are even stretching modes, identical to the lattice distortions achieved by Mn^{3+} ions in order to split the e_g electronic level (JT effect). It is therefore important to

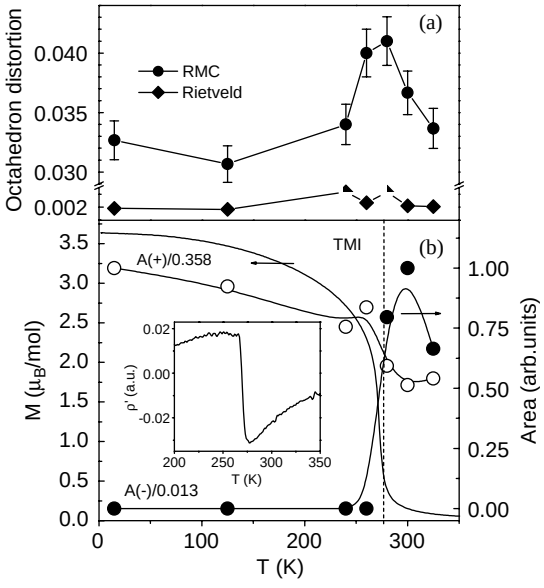

Fig. 7. (a) Temperature variation of the octahedron distortion from RMC and Rietveld results; and (b) temperature dependence of the magnetization (left axis); normalized integrated intensities (right axis) of the FM contribution to the spin correlation function, A(+), (○) and of the AF contributions to the spin–spin correlation functions, A(−), (•) of the spin correlations of NN Mn–Mn pairs. Inset shows the first derivative of the measured resistivity of LCMO.

identify these phonons and follow them through the different structural phases and doping levels.

Fig. 8 shows the strong dependence of the Raman spectra as the Ca content increases in the PM phases, at RT, of $La_{1-x}Ca_xMnO_3$ compounds. The width of the stretching mode peaks (symmetric stretching and Anti-symmetric stretching) increases and their intensity decreases and even disappears for substitutions at and above 50%. The drastic changes observed in a series of compounds with the same *Pnma* average structure can be understood in the following way: As the Ca content increases, the static cooperative JT distortion is reduced and the intensity of the high-frequency peaks decreases. But the Raman effect is a very rapid process so that the technique exploring the "instantaneous" atomic positions in the lattice, that are changing due to the polaron hopping, has to be considered. The instantaneous distribution of Mn–O distances is the origin of the width of these Raman peaks. The reduction of the activation energy for conduction in the PM phase when Ca content increases (Fig. 9) indicates that the binding

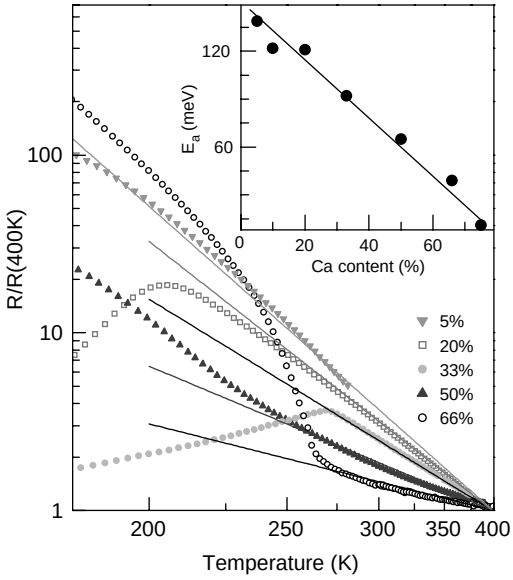

Fig. 9. Normalized resistance of samples with several Ca content. Lines are fits to the PM state resistance with: $R = R_0 \exp(E_a/K_B T)$. The inset shows the obtained activation energies E_a vs. Ca content.

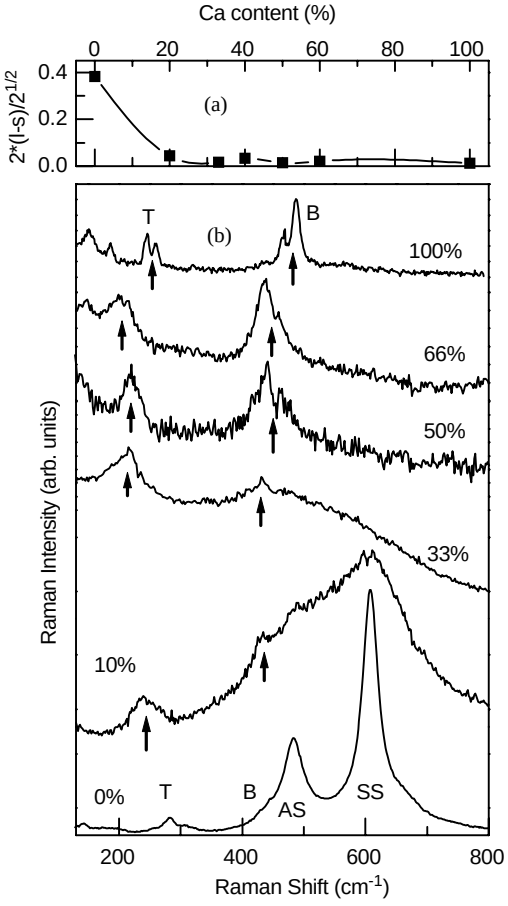

Fig. 8. (a) Cooperative static JT distortion, from diffraction for $La_{1-x}Ca_xMnO_3$ series; and (b) RT Raman spectra of $La_{1-x}Ca_xMnO_3$ samples, as function of Ca content. The arrows point the narrow peaks corresponding to the tilt and bending modes of the *R*-3*c* phase.

energy of the lattice polarons is decreasing. The reduction of the polaron energy implies the collapse of the amplitude of the dynamic distortions in the lattice. Therefore, for doping concentrations of 50% and above the lattice is, in fact, even instantaneously, much more regular than at low doping. As can be seen in the figure we then recover similar features to those appearing in the $CaMnO_3$ or LSMO type spectrum.

The spectrum corresponding to the insulating optimally Ca-doped $LaMnO_3$ can only be understood as a combination of two components. The narrow peaks indicated by arrows do not have the same origin as the broad features at high frequencies. These broadbands, which are similar to those of high-temperature $LaMnO_3$ where the JT orbital order is melt, correspond to the PM matrix with octahedra dynamically distorted by polaron hopping. The second kind of spectrum indicates that part of the sample has a structure similar to the metallic FM phase with regular MnO_6 octahedra. It very probably corresponds to the magnetic clusters or magnetic polarons discussed in the previous section. In the present context of phase segregation or inhomogeneous intrinsic phase in manganites, it is realistic to think that the second spectrum corresponds to FM metallic droplets in the PM matrix with polaronic (lattice polarons) conduction. At low temperatures, well in the FM metallic regime, the hopping carriers become delocalized and do not induce lattice distortions (Fig. 7). Only sharp phonon peaks are observed below 450 cm^{-1} as it occurs in $CaMnO_3$ and corresponds to MnO_6 octahedra with no static or dynamic distortions. The Raman spectra of the metallic

phases is independent of the averaged crystallographic structure: the same spectrum is observed for metallic *Pnma* LCMO or metallic *R*-3*c* LSMO at RT and at low temperature.

The identification of these types of spectra and their correspondence with particular octahedra configurations are the keys to understand the Raman spectra of most manganese perovskites. Moreover, this allows to detect the simultaneous presence of several different phases and to obtain insight in their local structure.

6. Intrinsic magnetoresistance and electron–phonon coupling

In order to obtain insight in the metallic–insulator transition in medium bandwidth systems, where the electron–phonon coupling is essential, we studied optimally Ca-doped (LCMO) epitaxial thin films with controlled chemical defects.

LCMO epitaxial films (thickness = 270 Å) were grown by dc sputtering on $SrTiO_3$ (100) substrates at room temperature. All films were annealed in O_2 at 800°C for 10 min. LCMO/Al_2O_3/LCMO trilayers were also obtained with different insulating layer thickness (between 6 and 100 Å) and always 270 Å thick LCMO.

The MR, at 5 K, is lower than 5% at 9 T for the discussed samples: a typical optimized LCMO sample (A), an oxygen-deficient film (B) and three trilayers (Al-6, Al-18 and Al-36, the number indicates the Al_2O_3 layer thickness in Å. For Al_2O_3 thickness up to 36 Å, the conduction is achieved through the contact regions between both LCMO layers.

The temperature dependence of the MR at low (0.5 T) and high (9 T) fields for the different samples is shown in Figs. 10a and b). Note that the changes in the MR at 9 T from one sample to the other have mainly occurred below 0.5 T. The maximum of the MR at 0.5 T occurs at temperatures lower than that of the high-field (9 T) MR which is closer to the metal–insulator transition T_{MI} (Fig. 11a). Fig. 10c presents the relative increase of the resistivity in the doped films compared to A sample vs. temperature at 0 T. The contribution of the impurities is basically limited to temperatures around T_c and below T_{MI} in coincidence with the maximum MR at 0.5 T, while not affecting the conductivity at low temperatures. This evidences that these low levels of chemical impurities are enhancing the localization of carriers below T_c. To a lesser extent this also occurs in "pure" LCMO (A sample). Polaron clusters form in the FM phase around T_c by the drastic reduction of the bandwidth due to lattice distortions around the defects. It is reasonable to think that these polarons are weakly bounded in the FM phase and therefore can be delocalized by a relatively weak field, explaining the unexpected component of the MR below 0.5 T. These

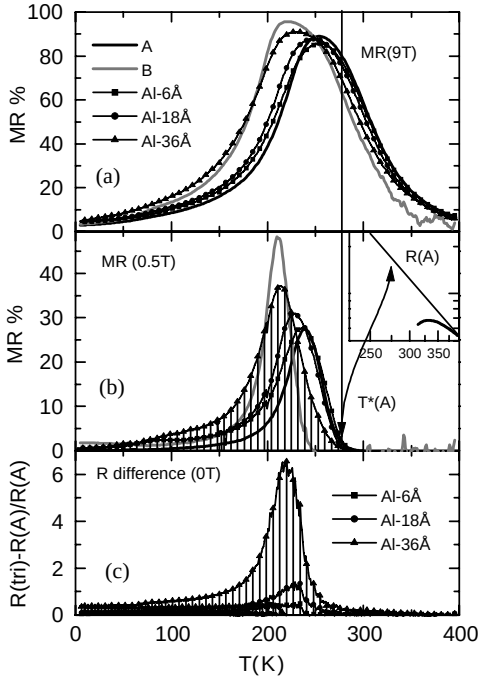

Fig. 10. Temperature dependence of (a) the MR at 9 T; (b) the MR (at 0.5 T) for the different samples; and (c) relative increase at 0 T of the resistivity $(R(\text{doped}) - R(A)/R(A))$ of Al-* samples compared to A film.

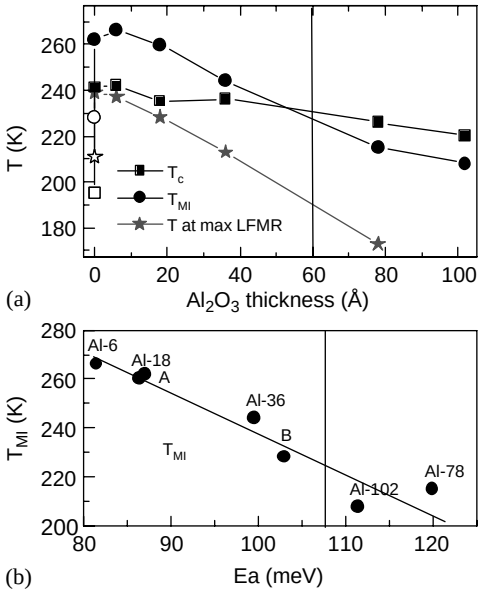

Fig. 11. (a) T_c, T_{MI} and temperature at which the MR at 0.5 T is maximum, open symbols correspond to B sample; and (b) T_{MI} vs. activation energy E_a.

small polarons can only be formed near T_c when the carrier bandwidth is reduced by (1) the spin disorder and (2) the lattice fluctuations. Fig. 11b shows the correlation between T_{MI} and the activation energy (E_a) for

conduction in the PM phase, which is proportional to the polaron binding energy (E_p). The lattice distortions around the defects favor the localization of the polarons (E_p increases). This becomes apparent in the PM phase as an increase of E_a and a decrease of the temperature at which metallic behavior is observed (T_{MI}), even maintaining T_c almost unchanged. A huge number of cases can be found in the literature showing that T_c and T_{MI} do not coincide. $T_{MI} < T_c$ occurs in polycrystalline or granular samples or films where the metallic conduction is hindered because of carrier scattering at grain boundaries and/or because of poor connectivity between grains, i.e., extrinsic effects. $T_{MI} > T_c$ is observed in single crystals, well-sintered pellets and epitaxial thin films. In the present case, this occurs for samples without structural barriers (up to Al-36). We conclude that in samples without grain boundaries the MI transition temperature is related to the electron–lattice interaction, which is increased by the introduction of chemical defects. Coming back to Fig. 10b, it is important to note that MR at 0.5 T begins to be significant at the temperature (T^*) at which the resistance deviates from the activated conduction (see inset) corresponding to polaron hopping. As mentioned above, at these temperatures percolation between metallic clusters occurs so the sample can be sketched as two resistances in parallel, one insulating and another metallic, with an effective section for metallic conduction that increases as the temperature decreases and/or as the magnetic field increases. It should be remarked that MR at 0.5 T is only observed when percolation is achieved (at T^*). This points out that it corresponds to a different process than the high-field MR that is already about its maximum at T^*. While high fields suppress spin fluctuations and induce magnetic order, low fields change the balance between localized and delocalized states. This effect can only be detected when percolation is achieved: a small increase in the size or number of disconnected metallic clusters (series equivalent circuit) does not change substantially the overall resistivity, while a small increase of the section of the low resistive metallic filaments can be detected as soon as percolation occurs.

7. Conclusions

We have reviewed the intrinsic and extrinsic contributions to the magnetoresistive properties of La–Ca manganites near the optimal doping. We have effectively modeled both contributions in terms of a two-channel model of resistances parallel connected. CB effects at low temperatures for nanometric grain sizes have been explicitly considered. We have searched for intrinsic inhomogneities, as predicted in the most recent theories, and have found definite evidence of the presence of phase segregation, form our neutron scattering results and Raman scattering experiments. Finally, we have shown that in samples without grain boundaries the MI transition temperature is related to the electron–lattice interaction which can be tuned by the introduction of chemical defects.

References

[1] J.M. Coey, M. Viret, S. Von Molnar, G. Blasse, A. Brill, Adv. Phys. 48 (1999) 167.
[2] E. Dagotto, T. Hotta, M. Moreo, Phys. Rep. 344 (2001) 1.
[3] A. de Andrés, M. García-Hernández, J.L. Martínez, Phys. Rev. B 60 (1999) 7328.
[4] A. de Andrés, M. García-Hernández, A. Muñoz-Martín, L. Martín, C. Prieto, L. Calzada, J.L. Martínez, Thin Solid Films. 373 (2000) 98.
[5] L. Martín-Carrón, R. Ramírez, C. Prieto, A. de Andrés, J. Sánchez-Benítez, M. García-Hernández, J.L. Martínez, J. Alloys Compounds 323 (2001) 527.
[6] M. García-Hernández, F. Guinea, A. de Andrés, J.L. Martínez, C. Prieto, L. Vázquez, Phys. Rev. B 61 (2000) 9549.
[7] M. García-Hernández, A. Mellergard, F. Mompeán, D. Sánchez, A. de Andrés, R.L. McGreevy, J.L. Martínez, Phys. Rev. Lett., cond-mat/0201436.
[8] A. de Andrés, S. Taboada, J.M. Colino, R. Ramírez, M. García-Hernández, J.L. Martínez, Appl. Phys. Lett. 81 (2002) 319.
[9] J.H. Park, E. Vescovo, H.J. Kim, C. Kwon, R. Ramesh, I. Venkatesan, Nature 392 (1998) 794.
[10] J.S. Helman, B. Abeles, Phys. Rev. Lett. 37 (1976) 1429.
[11] J.M. De Teresa, et al., Nature 386 (1997) 256.
[12] M. Fath, S. Freisem, A. Menovsky, Y. Tomioka, A. Aarts, J.A. Mydosh, Science 285 (1999) 1540.
[13] A. Mellergard, R.J. McGreevy, Acta Crystallogr. A 55 (1999) 783.
[14] P.G. Radaelli, D.E. Cox, M. Marezio, S.W. Cheong, P.E. Schiffer, A.P. Ramirez, Phys Rev. Lett. 75 (1995) 488.